J|A|C|S
ARTICLES
Published on Web 06/14/2002

Mono-Aromatic Ring-Fused versus *Adjacently* Di-Aromatic Ring-Fused Tetraazaporphyrins: Regioselective Synthesis and Their Spectroscopic and Electrochemical Properties

Nagao Kobayashi* and Takamitsu Fukuda

Contribution from the Department of Chemistry, Graduate School of Science, Tohoku University, Sendai 980-8578, Japan

Received October 17, 2001

Abstract: A method which preferentially produces *adjacently* di-aromatic ring-substituted tetraazaporphyrins (TAPs) has been developed, and their electrochemical and spectroscopic properties have been studied and compared with those of the corresponding series of mono-aromatic ring-fused TAPs. Mono-aromatic ring-fused TAPs show a split Q-band, and the splitting energy increases with increasing size of the aromatic ring. In addition, for the split Q-bands, the relative intensity of the band at longer wavelength decreases with increasing molecular size of the fused aromatics, compared with the shorter wavelength band. In the di-aromatic ring-fused TAPs, this kind of splitting is not seen, and only a shift of the band is observed. The intensity and band position of the split or unsplit Q-bands are quantitatively evaluated by simultaneous band deconvolution analysis, using both electronic absorption and magnetic circular dichroism spectra. The preparation of these TAP compounds has made it possible to adjust the Q-band position in a stepwise manner between ca. 600 and 750 nm. The first reduction and oxidation potentials of the TAP ring shift negatively with increasing number and size of the fused aromatics. The extent of the shift is found to be very small for the LUMOs but significant for the HOMOs. These spectroscopic and electrochemical properties are almost perfectly reproduced by molecular orbital calculations within the framework of the Pariser−Parr−Pople approximation. In particular, a small variation of the LUMO level and large destabilization of the HOMO level on ring expansion are rationalized from the extent of stretch of molecular orbitals: i.e., since the LUMOs are localized in the central TAP moiety irrespective of the molecular size, while the HOMOs have appreciable coefficients even over the fused aromatics, the HOMO level destabilizes while the LUMO level remains constant with increasing molecular size. In one CoTAP derivative, $Co^{III/II}$ and the first ligand oxidation couples occur experimentally at the same potential.

Introduction

Porphyrins and phthalocyanines (Pc's) are a very versatile class of compound. Since their structural confirmation in the early part of the 20th century,[1−3] numerous papers have been published, both in basic academic and in applied fields.[4−10] However, research on tetraazaporphyrins (TAPs), which are considered to be structural intermediates between normal porphyrins and Pc's,[11] become popular only about a decade ago, mainly because of the difficulty in preparing precursors and the low solubility of the resultant TAPs. In this respect, Hoffman's group developed the chemistry of TAPs intensively, particularly in the fields of synthesis and X-ray crystallographic analysis.[12] However, reports on spectroscopic analysis and electrochemical properties have been much less frequent. To

(1) Robertson, J. M.; Linstead, R. P.; Dent, C. E. *Nature* **1935**, *135*, 506.
(2) Linstead, R. P.; Robertson, J. M. *J. Chem. Soc.* **1936**, 1195.
(3) Crute, M. B. *Acta Crystallogr.* **1959**, *12*, 24.
(4) *Porphyrins and Metalloporphyrins*; Smith, K. M., Ed.; Elsevier: Amsterdam, 1975.
(5) *The Porphyrins*; Dolphin, D., Ed.; Academic Press: New York, 1978; Vols. 1−7.
(6) *The Porphyrin Handbook*; Kadish, K. M., Smith, K. M., Guilard, R., Eds.; Academic Press: New York, 1999.
(7) Lever, A. B. P. *Adv. Inorg. Chem. Radiochem.* **1965**, *7*, 27.
(8) *Phthalocyanines—Properties and Applications*; Leznoff, C. C., Lever, A. B. P., Eds.; VCH: New York, 1989 (Vol. 1), 1992 (Vol. 2), 1993 (Vol. 3), and 1996 (Vol. 4).
(9) *The Phthalocyanines*; Moser, F. H., Thomas, A. H., Eds.; CRC Press: Boca Raton, FL, 1983; Vols. 1 and 2.
(10) (a) De la Torre, G.; Claessens, C. G.; Torres, T. *Eur. J. Org. Chem.* **2000**, 2821. (b) *Phthalocyanines—Chemistry and Functions*; Shirai, H., Kobayashi, N., Eds.; IPC: Tokyo, 1997.
(11) (a) Kobayashi, N. In ref 8, Vol. 2, Chapter 3. (b) Kobayashi, N. In ref 6, Vol. 2, Chapter 13.
(12) (a) Michel, S. L. J.; Goldberg, D. P.; Stern, C.; Barrett, A. G. M.; Hoffman, B. M. *J. Am. Chem. Soc.* **2001**, *123*, 4741. (b) Lee, S.; White, A. J. P.; Williams, D. J.; Barrett, A. G. M.; Hoffman, B. M. *J. Org. Chem.* **2001**, *66*, 461. (c) Ehrlich, L. A.; Skrdla, P. J.; Jarrell, W. K.; Sibert, J. W.; Armstrong, N. R.; Saavedra, S. S.; Barrett, A. G. M.; Hoffman, B. M. *Inorg. Chem.* **2000**, *39*, 3963. (d) Bellec, N.; Montalban, A. G.; Williams, D. B. G.; Cook, A. S.; Anderson, M. E.; Feng, X.; Barrett, A. G. M.; Hoffman, B. M. *J. Org. Chem.* **2000**, *65*, 1774. (e) Montalban, A. G.; Jarrell, W.; Riguet, E.; McCubbin, Q. J.; Anderson, M. E.; White, A. J. P.; Williams, D. J.; Barrett, A. G. M.; Hoffman, B. M. *J. Org. Chem.* **2000**, *65*, 2472. (f) Nie, H.; Stern, C. L.; Barrett, A. G. M.; Hoffman, B. M. *Chem. Commun.* **1999**, 703. (g) Nie, H.; Barrett, A. G. M.; Hoffman, B. M. *J. Org. Chem.* **1999**, *64*, 6791. (h) Montalban, A. G.; Steinke, J. H. G.; Anderson, M. E.; Barrett, A. G. M.; Hoffman, B. M. *Tetrahedron Lett.* **1999**, *40*, 8151. (i) Andersen, K.; Anderson, M.; Anderson, O. P.; Baum, S.; Baumann, T. F.; Beall, L. S.; Broderick, W. E.; Cook, A. S.; Eichhorn, D. M.; Goldberg, D.; Hope, H.; Jarrell, W.; Lange, S. J.; McCubbin, Q. J.; Mani, N. S.; Miller, T.; Montalban, A. G.; Rodriguez-Morgade, M. S.; Lee, S.; Nie, H.; Olmstead, M. M.; Sabat, M.; Sibert, J. W.; Stern, C.; White, A. J. P.; Williams, D. B. G.; Williams, D. J.; Barrett, A. G. M.; Hoffman, B. M. *J. Heterocycl. Chem.* **1998**, *35*, 1013 and references therein. (j) Forsyth, T. P.; Williams, D. B. G.; Montalban, A. G.; Stern, C. L.; Barrett, A. G. M.; Hoffman, B. M. *J. Org. Chem.* **1998**, *63*, 331.

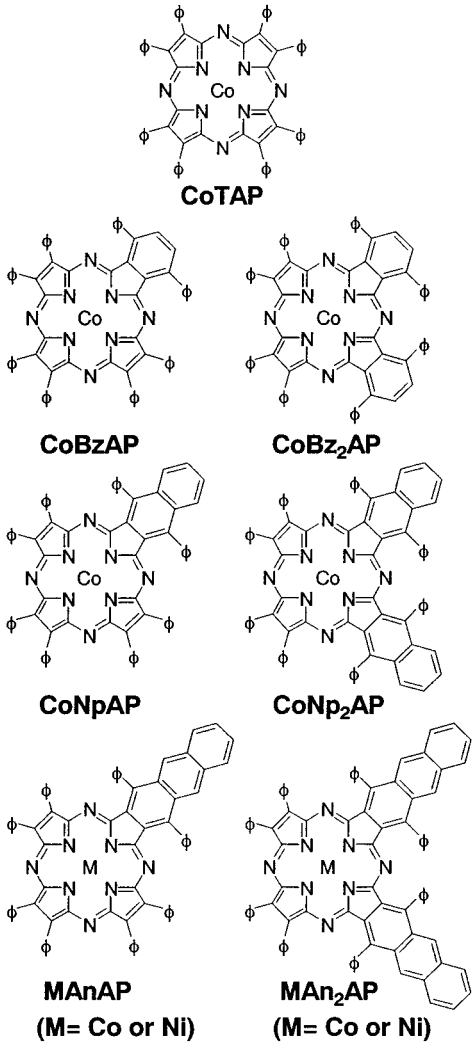

Figure 1. Structures and abbreviations of the compounds in this study.

our knowledge, no one has yet reported these kinds of properties on a series of TAP compounds of varying size. In one respect, this is due to the difficulty in controlling the structure of TAP compounds. Since low symmetrical TAPs can be obtained only by the mixed condensation of two kinds of maleonitrile or of a maleonitrile and aromatic ortho dinitriles, at least six types of product can possibly be formed, and the separation of these is not necessarily easy. In another respect, there is the difficulty in preparing a series of aromatic ortho dinitriles of a similar structure as one of the two starting precursors. To extract properties intrinsic to a series of compounds, we need to use similar compounds with similar substituents, and we hope they have sufficient solubility in a common solvent. For the TAP compounds, it was not easy to overcome these two difficulties. In this study, we have chosen diphenylmaleonitrile and 3,6-diphenylphthalonitrile, 2,3-dicyano-1,4-diphenylnaphthalene, or 2,3-dicyano-1,4-diphenylanthracene as precursors. Octaphenylated TAPs with D_{4h} symmetry generally have low solubility themselves, but we considered that eight phenyl groups may prevent the aggregation of low symmetrical TAPs obtained by a mixed condensation reaction, which is important for spectroscopic and theoretical studies. In addition, as shown in Figure 1, the phenyl groups in the compounds are at the same positions, precluding ambiguities in analysis, which makes our compounds ideal for the purpose of the present study. As described below, the finding of preferential formation of *adjacently* disubstituted TAP species has made this kind of study possible.

For the same reason described in the preceding paper (Kobayashi, N.; Miwa, H.; Nemykin, V. N., preceding paper in this issue), we chose cobalt as the central metal. Although zinc complexes are desirable from the standpoint of MO calculations and availability of both NMR and fluorescence spectroscopy, the naphtho-fused compounds were particularly unstable and could not be purified. On the other hand, low yields of nickel derivatives prevented the preparation of a series of this compound.

Experimental Section

(i) Measurements. The 400 MHz ^{1}H NMR and IR spectral measurements were made with JEOL GSX-400 and Shimadzu FTIR-8100M spectrometers, respectively. Mass spectra were measured with a Hitachi M-2500S spectrometer (EI mass) and with a JEOL JMS-HX110 mass spectrometer (FAB mass) using *m*-nitrobenzyl alcohol (NBA) as a matrix. Electronic absorption spectra were measured with a Hitachi U-3410 spectrophotometer. Magnetic circular dichroism (MCD) spectra were run on a Jasco J-725 spectrodichrometer using a toluene solution of ca. $10^{-5}-10^{-6}$ mol/L, with a Jasco electromagnet that produced a magnetic field of up to 1.09 T. The magnitude of this was expressed in terms of molar ellipticity per tesla, $[\theta]_M$/deg mol^{-1} dm^3 cm^{-1} T^{-1}.

Cyclic voltammetry data were collected with a Hokuto Denko HA-501 potentiostat connected to a Graphtec WX1200 *XY* recorder. Differential pulse voltammetry data were recorded with a Yanaco P-1100 polarographic analyzer connected to a Watanabe WX 4401 *XY* recorder. Electrochemical experiments were performed under purified nitrogen gas. A glassy carbon working electrode (area = 0.07 cm^2) and a Pt wire counter electrode were employed. The reference electrode was Ag/AgCl, corrected for junction potentials by being referenced internally to the ferrocenium/ferrocene (Fc^+/Fc) couple. In the solution used, i.e., in *o*-dichlorobenzene (*o*-DCB, Nacalai Tesque, HPLC grade) containing 0.1 mol/L tetrabutylammonium perchlorate (TBAP), the Fc^+/Fc couple was observed at 0.51 ± 0.02 V vs Ag/AgCl. For spectroelectrochemical measurements, an optically transparent thin-layer electrode (OTTLE) cell of path length 1 mm was employed using a Pt minigrid as both working and counter electrodes[13] and a TBAP concentration of 0.3 mol/L.

(ii) Molecular Orbital Calculations. MO calculations were performed by the ZINDO/S Hamiltonian in the HyperChem R.5.1 program[14a] and the Pariser−Parr−Pople (PPP) Hamiltonian described previously.[14b] The structures of Pc analogues for calculations were constructed by using X-ray structural data of standard Pc,[15] naphthalene,[16a] and anthracene[16b] and by making the rings perfectly planar and adopting the C_{2v} symmetry, and therefore essentially the same as those we used in our previous papers.[17] The central metal was assumed as zinc for the ZINDO/S calculations and nil for the PPP calculations. The choice

(13) Kobayashi, N.; Nishiyama, Y. *J. Phys. Chem.* **1985**, *89*, 1167.
(14) (a) *HyperChem R.5.1 Pro*; Hypercube Inc., Gainesville, FL, 1997. (b) Tokita, S.; Matsuoka, K.; Kogo, Y.; Kihara, K. *Molecular Design of Functional Dyes-PPP Method and Its Application*; Maruzen: Tokyo, 1990.
(15) Robertson, J. M.; Woodward, I. *J. Chem. Soc.* **1937**, 219. Barrett, P. A.; Dent, C. E.; Linstead, R. P. *J. Chem. Soc.* **1936**, 1719. Brown, C. J. *J. Chem. Soc. A* **1968**, 2488, 2494. Kirner, J. F.; Dow, W.; Scheidt, D. R. *Inorg. Chem.* **1976**, *15*, 1685.
(16) (a) House, H. O.; Koepsell, D. G.; Campbell, W. J. *J. Org. Chem.* **1972**, *37*, 1003. (b) Fillers, J. P.; Ravichsandran, K. G.; Abdalmuhdi, I.; Chang, C. K. *J. Am. Chem. Soc.* **1986**, *108*, 417.
(17) (a) Gouterman, M. *J. Mol. Spectrosc.* **1961**, *6*, 138. (b) Kobayashi, N.; Konami, H. In *Phthalocyanines—Properties and Applications*; Leznoff, C. C., Lever, A. B. P., Eds.; VCH: New York, 1996; Vol. 4, Chapter 13. (c) Kobayashi, N.; Konami, H. *J. Porphyrins Phthalocyanines* **2001**, *5*, 233. (d) Kobayashi, N.; Ishizaki, T.; Ishii, K.; Konami, H. *J. Am. Chem. Soc.* **1999**, *121*, 9096.

of configuration was based on energetic considerations, and all singly excited configurations up to 9 eV (72 590 cm^{-1}) were included.

(iii) Synthesis. All new low symmetrical TAPs in Figure 1 have been obtained by mixed condensation between diphenylmaleonitrile[18] and either 3,6-diphenylphthalonitrile,[19a] 2,3-dicyano-1,4-diphenylnaphthalene,[19b,c] or 2,3-dicyano-1,4-diphenylanthracene. Yields of the TAP derivatives were calculated on the basis of the total nitrile mixed.

2,3-Dicyano-1,4-diphenyl-1,4-oxide-2,3-dihydroanthracene. To 10 mL of dichloromethane containing 6.3 g (20 mmol) of 1,3-diphenylnaphtho[*2,3-c*]furan[20] was added fumaronitrile stepwise with stirring until the solution changed from red to yellow. The solvent was evaporated and the residue recrystallized from methanol, to give 7.2 g (90%) of the desired product, mp 214−217 °C. Mass (EI) (*m*/*z*): 398 (M^+). IR (KBr): 2338, 2365 cm^{-1} (CN). ^{1}H NMR ($CDCl_3$, 400 MHz): δ 3.69 (d, 1H), 3.97 (d, 1H), 7.50−7.68 (m, 10H), 7.73 (d, 2H), 7.78−7.82 (m, 2H), 7.88 (d, 2H). ^{13}C NMR ($CDCl_3$, 100 MHz): δ 18.2, 58.3, 71.9, 83.7, 126.4, 127.5, 128.0, 128.1, 128.6, 129.8, 130.9, 131.6, 132.6, 141.2, 147.0, 147.1. Anal. Found: C, 84.36; H, 4.58; N, 6.99. Calcd for $C_{28}H_{18}N_2O$: C, 84.40; H, 4.55; N, 7.03.

2,3-Dicyano-1,4-diphenylanthracene. The above compound (7.2 g, 18 mmol) was added to 5 mL of concentrated sulfuric acid and stirred for 10 min at 0 °C. The reaction mixture was poured into ice and stirred for a further 20 min, and then the precipitated solid was filtered off and washed with water and methanol. Recrystallization from CH_2Cl_2 gave 6.5 g (94%) of the desired compound. mp > 320 °C. Mass (EI) (*m*/*z*): 380 (M^+). IR (KBr): 2226 cm^{-1} (CN). ^{1}H NMR ($CDCl_3$, 400 MHz): δ 7.55−7.58 (m, 6H), 7.63−7.66 (m, 6H), 7.91−7.94 (dd, 2H), 8.34 (s, 2H). ^{13}C NMR ($CDCl_3$, 100 MHz): δ 108.5 (^{13}C−CN), 116.1 (C−^{13}CN), 128.2, 128.6, 128.8, 129.1, 129.7, 129.9, 130.0, 133.3, 135.6, 149.1. Anal. Found: C, 88.41; H, 4.22; N, 7.37. Calcd for $C_{28}H_{16}N_2$: C, 88.40; H, 4.24; N, 7.36.

[2,3,7,8,12,13,17,18-Octaphenyl-5,10,15,20-tetraazaporphyrinato-(2−)]cobalt(II), CoTAP. This compound was prepared in 50% yield according to the literature.[18] Mass (FAB) (*m*/*z*): 980 ($M^+ + 1$). Anal. Found: C, 77.70; H, 4.92; N, 11.08. Calcd for $C_{64}H_{40}N_8Co$: C, 78.44; H, 4.11; N, 11.43.

[2^1,2^4-Diphenylbenzo[*b*]-7,8,12,13,17,18-hexaphenyl-5,10,15,20-tetraazaporphyrinato(2−)]cobalt(II), CoBzAP, and [2^1,2^4,7^1,7^4-Tetraphenyldibenzo[*b*,*g*]-12,13,17,18-tetraphenyl-5,10,15,20-tetraazaporphyrinato(2−)]cobalt(II), CoBz$_2$AP. To 3 mL of 1-hexanol solution containing ca. 20 mg (2.9 mmol) of lithium was added a mixture of finely powdered diphenylmaleonitrile (299 mg, 1.30 mmol) and 3,6-diphenylphthalonitrile (314 mg, 1.12 mmol), and the solution was stirred at 140 °C for 1 h. Most of the solvent was removed by passing nitrogen gas over the solution at this temperature, and then 20 mL of DMF and anhydrous cobalt(II) chloride (2.9 g, 22 mmol, 36 equiv) were added, and the stirring was continued for a further 30 min at this temperature. After cooling, the solution was poured into 200 mL of water, and the resultant precipitate was collected by filtration and washed with water and methanol. After drying, the crude product was repeatedly imposed on a silica gel column followed by a preparative thin-layer (PLC, silica) plate using carbon tetrachloride/toluene (1:1 v/v) as eluent, and the portions with R_f = 0.50 ($CoBz_2AP$) and 0.33 (CoBzAP) were collected. Recrystallization from dichloromethane/methanol produced the desired CoBzAP (7.7 mg, 1.2%) and $CoBz_2AP$ (54 mg, 8.3%) as a blue solid. Mass (FAB) (*m*/*z*): 1030 ($M^+ + 1$ for CoBzAP), 1080 ($M^+ + 1$ for $CoBz_2AP$). Anal. Found: C, 77.77; H, 5.13; N, 10.04. Calcd for $C_{68}H_{42}N_8Co\cdot H_2O$ (CoBzAP): C, 77.93; H, 4.23; N, 10.69. Anal. Found: C, 79.89; H, 4.33; N, 10.29. Calcd for $C_{72}H_{44}N_8Co$ ($CoBz_2AP$): C, 80.06; H, 4.11; N, 10.37.

[2^1,2^6-Diphenylnaphtho[*b*]-7,8,12,13,17,18-hexaphenyl-5,10,15,20-tetraazaporphyrinato(2−)]cobalt(II), CoNpAP, and [2^1,2^6,7^1,7^6-Tetraphenyldinaphtho[*b*,*g*]-12,13,17,18-tetraphenyl-5,10,15,20-tetraazaporphyrinato(2−)]cobalt(II), CoNp$_2$AP. As for the above CoBzAP and $CoBz_2AP$, these were synthesized from diphenylmaleonitrile (330 mg, 1.43 mmol) and 2,3-dicyano-1,4-diphenylnaphthalene (372 mg, 1.13 mmol). The crude reaction product was purified using a PLC plate on silica with toluene as eluent. Two fractions with R_f = 0.85 ($CoNp_2AP$) and 0.65 (CoNpAP) were collected and recrystallized from dichloromethane/methanol, to give 23 mg (3.3%) of CoNpAP as a blue solid and 82 mg (11%) of $CoNp_2AP$ as a green solid. Mass (FAB) (*m*/*z*): 1080 ($M^+ + 1$ for CoNpAP), 1180 ($M^+ + 1$ for $CoNp_2AP$). Anal. Found: C, 80.19; H, 4.24; N, 10.43. Calcd for $C_{72}H_{44}N_8Co$ (CoNpAP): C, 80.06; H, 4.11; N, 10.37. Anal. Found: C, 80.56; H, 4.38; N, 9.34. Calcd for $C_{80}H_{48}N_8Co$ ($CoNp_2AP$): C, 81.41; H, 4.10; N, 9.49.

[2^1,2^8-Diphenylanthraco[*b*]-7,8,12,13,17,18-hexaphenyl-5,10,15,20-tetraazaporphyrinato(2−)]cobalt(II), CoAnAP, and [2^1,2^8,7^1,7^8-Tetraphenyldianthraco[*b*,*g*]-12,13,17,18-tetraphenyl-5,10,15,20-tetraazaporphyrinato(2−)]cobalt(II), CoAn$_2$AP. To 5 mL of 1-hexanol containing ca. 100 mg (14 mmol) of lithium was added a mixture of finely powdered diphenylmaleonitrile (180 mg, 0.78 mmol) and 2,3-dicyano-1,4-diphenylanthracene (250 mg, 0.66 mmol), and the solution was stirred at 150 °C for 1 h. Most of the solvent was removed by passing nitrogen gas over the solution at this temperature, and then 30 mL of DMF and anhydrous cobalt(II) chloride (1.4 g, 11 mmol, 31 equiv) were added, and the stirring continued for 30 min more at this temperature. After cooling, the solution was poured into 200 mL of water, and the resultant precipitate was collected by filtration and washed with water and methanol. The crude reaction product was purified using a PLC plate on silica with toluene as eluent, and two portions with R_f = 0.83 ($CoAn_2AP$) and 0.68 (CoAnAP) were collected. Recrystallization from dichloromethane/methanol produced the desired CoAnAP (16 mg, 3.9%) as a blue solid and $CoAn_2AP$ (40 mg, 8.7%) as a green solid. Mass (FAB) (*m*/*z*): 1130 ($M^+ + 1$ for CoAnAP), 1280 ($M^+ + 1$ for $CoAn_2AP$). Anal. Found: C, 80.45; H, 4.44; N, 10.00. Calcd for $C_{76}H_{46}N_8Co$ (CoAnAP): C, 80.77; H, 4.10; N, 9.91. Anal. Found: C, 81.98; H, 4.33; N, 8.65. Calcd for $C_{88}H_{52}N_8Co$ ($CoAn_2AP$): C, 82.55; H, 4.09; N, 8.75.

[2^1,2^8-Diphenylanthraco[*b*]-7,8,12,13,17,18-hexaphenyl-5,10,15,20-tetraazaporphyrinato(2−)]nickel(II), NiAnAP, and [2^1,2^8,7^1,7^8-Tetraphenyldianthraco[*b*,*g*]-12,13,17,18-tetraphenyl-5,10,15,20-tetraazaporphyrinato(2−)]nickel(II), NiAn$_2$AP. These compounds were obtained using nickel(II) chloride instead of cobalt(II) chloride in the preparation of CoAnAP and $CoAn_2AP$, to confirm the structure from ^{1}H NMR and to investigate the spectroelectrochemistry of ring-reduced and -oxidized species. The yield of blue colored NiAnAP and reddish brown $NiAn_2AP$ was 4 mg (0.9%) in both cases, this low yield being attributable to reduction in the purification process due to low solubility. Mass (FAB) (*m*/*z*): 1129 ($M^+ + 1$ for NiAnAP), 1279 ($M^+ + 1$ for $NiAn_2AP$). Anal. Found: C, 80.87; H, 4.12; N, 9.74. Calcd for $C_{76}H_{46}N_8Ni$ (NiAnAP): C, 80.79; H, 4.10; N, 9.92. Anal. Found: C, 82.09; H, 4.27; N, 8.69. Calcd for $C_{88}H_{52}N_8Ni$ ($NiAn_2AP$): C, 82.57; H, 4.09; N, 8.75. ^{1}H NMR ($CDCl_3$, 400 MHz): for NiAnAP, δ 7.07−7.15 (m, 2H), 7.27−7.31 (dd, 4H), 7.38−7.50 (m, 26H), 7.60−7.62 (d, 4H), 7.84−7.89 (m, 4H), 7.93−7.96 (m, 2H), 8.06−8.13 (m, 4H), 8.53 (s, 2H); for $NiAn_2AP$, δ 7.10−7.55 (m, 40H), 7.73−7.76 (m, 4H), 7.85−7.92 (m, 4H), 8.35 (s, 2H), 8.61 (s, 2H).

Results and Discussion

(i) Synthesis. As described above, from the condensation reaction using two kinds of ortho dinitriles in a 1:1 ratio, only adjacently di-aromatic-ring fused (AABB type) and mono-aromatic ring-fused (ABBB type) species were obtained, and the preferential formation of the former was confirmed (roughly

(18) Cook, A. H.; Linstead, R. P. *J. Chem. Soc.* **1937**, 929.
(19) (a) Kobayashi, N.; Ashida, T.; Osa, T. *Chem. Lett.* **1992**, 1567, 2031. (b) Kobayashi, N.; Ashida, T.; Osa, T.; Konami, H. *Inorg. Chem.* **1994**, *33*, 1735. (c) Kobayashi, N.; Togashi, M.; Osa, T.; Ishii, K.; Yamauchi, S.; Hino, H. *J. Am. Chem. Soc.* **1996**, *118*, 1073.
(20) Cava, M. P.; VanMeter, J. P. *J. Org. Chem.* **1969**, *34*, 538.

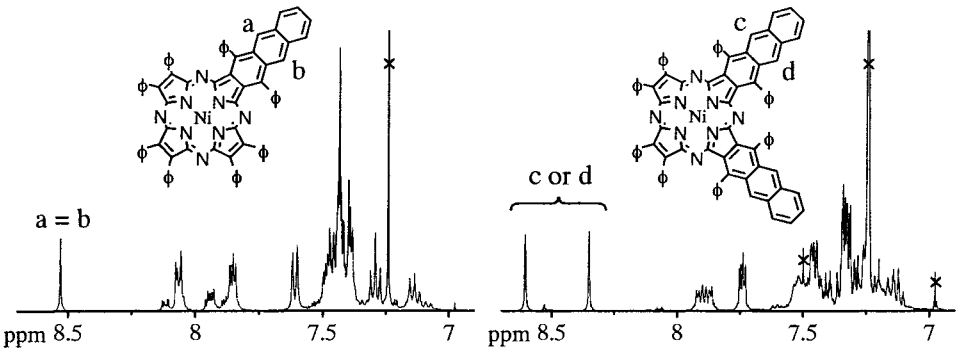

Figure 2. 400 MHz ^{1}H NMR spectra of NiAnAP (left) and $NiAn_2AP$ (right) in $CDCl_3$. In the spectra of $NiAn_2AP$, a small amount of NiAnAP was intentionally added in order to increase the solubility. Signals from the solvent are marked X.

3−7 times). The key factor in the synthesis was the use of lithium at the first stage, so that the subsequent addition of transition metals produced the above results. If transition metals were used from the beginning, no AABB type compounds would be obtained.[19] From experiments carried out under various conditions, we have explained the above results as follows. Lithium acts as a strong template, so that initially two dinitriles containing two protruding phenyl groups such as 3,6-diphenylphthalonitrile react to form a half Pc,[21] after which it will become harder for another 3,6-diphenylphthalonitrile to link to this unit due to steric hindrance of the phenyl groups. In particular, lithium is the hardest metal in the soft−hard concept (i.e., small volume but high charge density), so that when two dinitrile molecules, say 3,6-diphenylphthalonitrile, are connected by lithium to form a half Pc, these molecules are considered to take a folded conformation around lithium, thereby making the attack of the third dinitrile difficult. Of course, at higher temperature, the third dinitrile may be able to link to this half Pc,[22] but by controlling the reaction temperature, it is possible to stop further addition of the sterically hindered diphenylphthalonitrile. Diphenylmaleonitrile then reacts at slower rate to form a half Pc, because of the absence of a unit to keep the dinitrile moiety flat (in phthalonitrile, for example, two nitrile units are kept flat by the presence of a benzene ring, which makes coordination to template metals easier, thereby facilitating the formation of the Pc skeleton). In this study, we used diphenylmaleonitrile as one of the precursors because of the easy accessibility,[18] and therefore octaphenyltetraazaporphyrin was also formed. However, because of its low solubility in various solvents, this compound was easily removed during column chromatography.

Figure 2 shows ^{1}H NMR spectra of NiAnAP and $NiAn_2AP$ specially prepared for this purpose. As expected for the structures of these compounds, the protons at the center of anthracene moiety appear as a singlet for NiAnAP and two separate singlets for $NiAn_2AP$, confirming the desired structures.[23]

(ii) Electronic Absorption and MCD Spectroscopy. Figure 3 shows the absorption and MCD spectra of NiAnAP and $NiAn_2AP$ recorded in order to look for any correlation with the above NMR results. According to the symmetry-adapted perturbation (SAP) theory,[17a,b] NiAnAP and $NiAn_2AP$ should

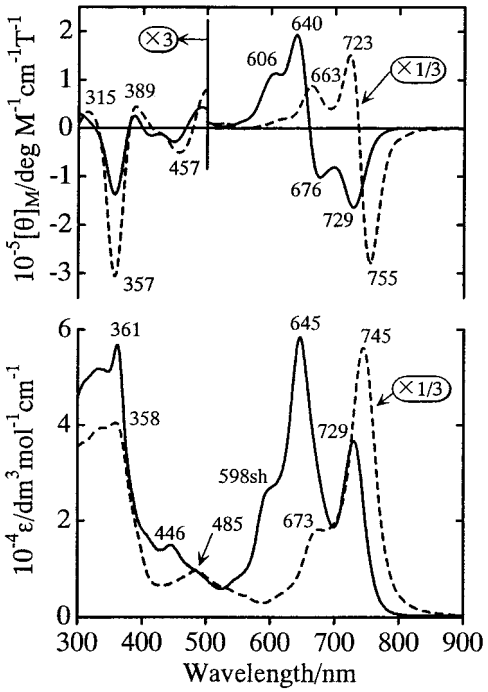

Figure 3. Electronic absorption (bottom) and MCD spectra (top) of NiAnAP (solid lines) and $NiAn_2AP$ (broken lines) in toluene. Note the encircled magnification factor.

show a split and unsplit Q-band, respectively, and the Q-band position of the latter should appear at longer wavelength than the former. Indeed, the anticipated spectra were observed, and the corresponding MCD spectra were also consistent with the structure, i.e., Faraday *B*-term type and *A*-term type, respectively.[24] Although the structure and spectral shape relationship was as expected, of particular note is the large intensity difference between NiAnAP and $NiAn_2AP$. As indicated by the encircled magnification factor in the figure, the intensity of $NiAn_2AP$ is much higher than that of NiAnAP. However, this is also consistent with the MO calculation result, that the intensity of the Q-band of TAP increases markedly with fusing of large aromatic molecules.[17a−c] The small absorption peaks seen at 446 and 485 nm can be ascribed to transitions in anthracene-centered orbitals.[17b,25]

Figure 4A and B displays electronic absorption and MCD spectra, respectively, of ABBB type cobalt species in toluene.

(21) Nolan, K. J. M.; Hu, M. J.; Leznoff, C. C. *Synlett* **1997**, 593.
(22) Kobayashi, N.; Fukuda, T.; Ueno, K.; Ogino, H. *J. Am. Chem. Soc.* **2001**, *123*, 10740.
(23) The structure of $CoAn_2AP$ has also been confirmed by X-ray crystallography.[22]
(24) Stillman, M. J.; Nyokong, T. In *Phthalocyanines—Properties and Applications*; Leznoff, C. C., Lever, A. B. P., Eds.; VCH: New York, 1989; Vol. 1, Chapter 3.
(25) Miwa, H.; Kobayashi, N. *Chem. Lett.* **1999**, 1303.

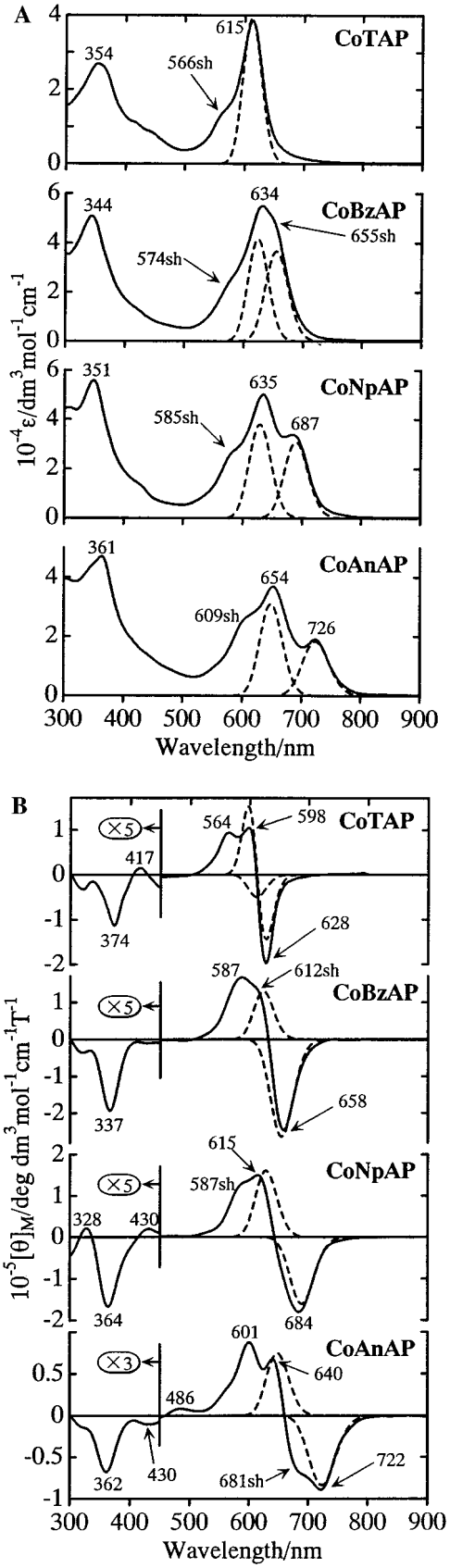

Figure 4. (A) Electronic absorption and (B) MCD spectra of CoTAP, CoBzAP, CoNpAP, and CoAnAP in toluene. Note the encircled magnification factor in (B). The Gaussian lines drawn by broken lines indicate a split Q_{00}-band by band deconvolution analysis.

As exemplified by the above NiAnAP, all these complexes show split Q-bands, and the splitting increases with increasing size of the fused aromatics. Of the split Q-bands, the band at shorter wavelength shows little or no change in its position, while that at longer wavelength shifts to the red with a concomitant decrease in relative intensity. If we consider the center of the split Q-band as the position of the Q-band of the ABBB type species, the shifts from the Q-band of CoTAP are 680, 1130, and 1710 cm^{-1} for CoBzAP, CoNpAP, and CoAnAP, respectively, based on band deconvolution analysis. Thus, the energy differences (ΔE) for CoTAP−CoBzAP, CoBzAP−CoNpAP, and CoNpAP−CoAnAP are 680, 450, and 580 cm^{-1}, respectively. The Soret band position shifts to shorter wavelength on going from CoTAP to CoBzAP, but then it shifts to longer wavelength with increasing molecular size; i.e., the energy difference between CoBzAP and CoNpAP is 580 cm^{-1}, while that between CoNpAP and CoAnAP is 790 cm^{-1}. In this way, ΔE values in the Soret band are not particularly small compared with those in the Q-band. All compounds show a curvature at the foot of the longer wavelength tail of the Soret band, suggesting there is at least one other transition in this region. The MCD spectra show dispersion type curves in the Q-band region, roughly corresponding to the split absorption peaks. These are therefore interpreted as a superimposition of Faraday *B*-terms.[26] However, since the splitting is not large enough to be observed as separate peaks, particularly for CoBzAP and CoNpAP, they look apparently like Faraday *A*-terms (*pseudo A*-term).[27] Similarly to the case with normal TAPs and Pc's with D_{4h} symmetry,[24] the intensity in the Soret band region is much weaker than that in the Q-band, reflecting the ΔL (angular momentum) $= \pm 1$ nature of the former compared with $\Delta L = \pm 9$ of the latter.

Figure 5A and B shows spectra for adjacently disubstituted AABB type compounds. With increasing size of the fused aromatics, the Q-band shifts to longer wavelength without appreciable splitting. The position of the Q-band lies always at longer wavelength, while the Soret band lies at shorter wavelength than in the corresponding monosubstituted ABBB type species in Figure 4A. The shift of the Q-band from the Q-band of CoTAP is approximately twice as large as that in the case of the corresponding monosubstituted ABBB type compounds, as has been anticipated by the SAP method.[17a,b] For example, the ΔE values of CoTAP−CoBz$_2$AP and CoTAP−CoNp$_2$AP are 1390 and 2230 cm^{-1}, respectively, while $\Delta E =$ 680 and 1130 cm^{-1} for CoTAP−CoBzAP and CoTAP−CoNpAP, respectively. One or two small curvatures are discernible at the foot of the red tail of the Soret band envelope. The MCD spectra of all compounds are dispersion type Faraday *A*-terms corresponding to the Q absorption peaks, suggesting the presence of degenerate excited states. In the Soret band region, there appear to be several transitions since curves are not simple and appear to be a superimposition of several Faraday *A*-terms.

The absorption and MCD data of all the compounds in this study are summarized in Table 1. As can be seen in this table and Figures 4A and 5A, it becomes possible to adjust the main absorption band (i.e., Q-band) of TAPs stepwise over the wide region ranging ca. 600−750 nm. In the case of ABBB type compounds, the bands are broad, but for AABB type com-

(26) Tajiri, A.; Winkler, J. *Z. Naturforsch.* **1983**, *38a*, 1263.
(27) Kaito, A.; Nozawa, T.; Yamamoto, T.; Hatano, M.; Orii, Y. *Chem. Phys. Lett.* **1977**, *52*, 154.

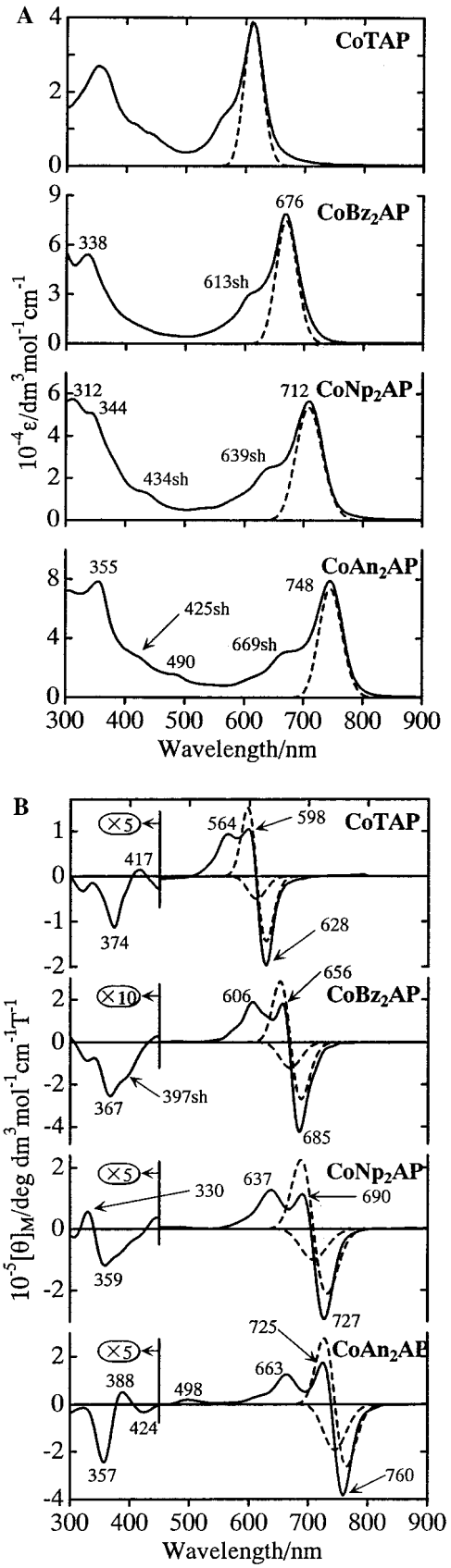

Figure 5. (A) Electronic absorption and (B) MCD spectra of CoTAP, $CoBz_2AP$, $CoNp_2AP$, and $CoAn_2AP$ in toluene. Note the encircled magnification factor in (B). The Gaussian lines shown by broken lines indicate a Q_{00}-band obtained by band deconvolution analysis.

pounds, the Q-band width does not change significantly from species to species.

Deconvolution of the spectroscopic envelope can give reliable results if both the absorption and MCD spectra are fitted with the same or very similar band centers and bandwidth parameters. In fact, to date, many absorption and MCD spectra have been analyzed by band deconvolution, and this has been successful in analyzing transitions that had been postulated by MO calculations or in finding a new degenerate excited state.[28] We have therefore employed this method in order to obtain quantitative information. Figure 6 shows an example of band deconvolution analysis for the Q-band of CoAnAP. In this figure, the two obtained Q_{00}-bands are indicated by solid lines. Deviation of the simulated spectrum from that obtained experimentally is very small, as shown at the bottom of the figure. The Q-bands of the other compounds have been similarly analyzed, with the obtained parameters summarized in Table 2, and the Q_{00} components are added in Figures 4 and 5 as broken lines. In the case of monosubstituted ABBB type compounds shown in Figure 4A and B, two components are required in both the absorption and MCD spectra. In the case of absorption spectra of Figure 4A, splitting of the Q-band increases and the relative intensity of the component at longer wavelength decreases with increasing size of the fused aromatics. For adjacently disubstituted AABB type compounds, only one component is required in the Q-band region (Figure 5). The Q-band MCD is expressed by a single Faraday *A*-term. Since Gaussian curves are used for the deconvolution analysis, parameters of each envelope are accurately obtained (Table 2). For example, absorption coefficients, band positions, oscillator strengths, and so forth are numerically expressed, and these are used in the comparison of the results of the MO calculations.

(iii) Electrochemistry. Redox potentials have been reported for many Pc's[29] and porphyrins.[30] In particular, the first oxidation and reduction potentials are important for finding the relationship between the absorption bands lying at the longest wavelength. Figure 7 displays the cyclic voltammograms of cobalt complexes in *o*-DCB containing 0.1 mol/L TBAP, while the data are collected in Table 3 and Figure 8. The oxidation potential of CoBzAP was read from the differential pulse voltammogram, and the second oxidation potential of $CoNp_2$-AP was not obtained because of the instability of the first oxidation product. TAP derivatives fused with naphthalene rings such as some types of naphthalocyanine[31] and tribenzomononaphthoTAP[32] are experimentally known to be unstable with respect to oxidation, and the above data are consistent with this. From the difference between the various redox potentials, all processes except for the first oxidation of CoTAP and CoBzAP are one-electron processes. The first oxidation curve of CoTAP was found to be a superimposition of two oxidation curves, since two peaks appeared at higher scans, of which the more positive peak became more prominent at higher scan rates.

(28) Some examples: Nyokong, T.; Gasyna, Z.; Stillman, M. J. *Inorg. Chem.* **1987**, *26*, 1087. Browett, J. R.; Stillman, M. J. *J. Am. Chem. Soc.* **1988**, *110*, 3633. Ough, E.; Nyokong, T.; Kreber, K. A.; Stillman, M. J. *Inorg. Chem.* **1988**, *27*, 2724. Ough, E. A.; Stillman, M. J. *Inorg. Chem.* **1994**, *33*, 573. Mack, M. J.; Stillman, M. J. *J. Am. Chem. Soc.* **1994**, *116*, 1292. Kobayashi, N.; Fukuda, T.; Lelièvre, D. *Inorg. Chem.* **2000**, *39*, 3632.
(29) Lever, A. B. P.; Milaeva, E. R.; Speier, G. In *Phthalocyanines—Properties and Applications*; Leznoff, C. C., Lever, A. B. P., Eds.; VCH: New York, 1993; Vol. 3.
(30) Kadish, K. M.; Royal, G.; Caemelbecke, E. V.; Gueletti, L. In *The Porphyrin Handbook*; Kadish, K. M., Smith, K. M., Guilard, R., Eds.; Academic Press: New York, 1999; Chapter 59.
(31) Kobayashi, N.; Higashi, Y.; Osa, T. *Chem. Lett.* **1994**, 1813.
(32) Kobayashi, N.; Kondo, R.; Nakajima, S.; Osa, T. *J. Am. Chem. Soc.* **1990**, *112*, 9640.

Table 1. Absorption and MCD Data in Toluene

compound	absorption[a]		MCD[b]		
CoTAP	354 (2.69)	566sh[c] (1.42)	374 (−0.23)	417 (0.03)	564 (0.93)
	615 (3.83)		598 (1.04)	628 (−1.98)	
CoBzAP	344 (5.09)	574sh (2.36)	337 (−0.06)	587 (1.66)	612sh (1.37)
	634 (5.48)	655sh (4.61)	658 (−2.45)		
CoNpAP	351 (5.56)	585sh (2.72)	328 (0.04)	364 (−0.33)	430 (0.04)
	635 (5.01)	687 (3.35)	587sh (1.29)	615 (1.50)	684 (−1.80)
CoAnAP	361 (4.69)	609sh (2.67)	362 (−0.23)	430 (−0.04)	486 (0.08)
	654 (3.68)	726 (1.88)	601 (0.87)	640 (0.66)	681sh (−0.65)
			722 (−0.89)		
$CoBz_2AP$	338 (5.39)	613sh (3.12)	367 (−0.25)	397sh (−0.16)	606 (1.87)
	676 (7.27)		656 (1.80)	685 (−4.25)	
$CoNp_2AP$	312 (5.74)	344 (5.06)	330 (0.11)	359 (−0.24)	637 (1.27)
	434sh (1.30)	639sh (2.46)	690 (1.12)	727 (−2.93)	
	712 (5.61)				
$CoAn_2AP$	355 (7.83)	425sh (2.69)	357 (−0.49)	388 (0.10)	424 (−0.07)
	490 (1.48)	669sh (3.06)	498 (0.19)	663 (1.26)	725 (1.75)
	748 (7.82)		760 (−3.83)		
NiAnAP	361 (5.68)	446 (1.49)	357 (−0.46)	387 (0.08)	410 (−0.05)
	598sh (2.66)	645 (5.82)	450 (−0.10)	490 (0.14)	527 (0.03)
	729 (3.66)		606 (1.13)		
$NiAn_2AP$	358 (12.1)	485 (2.87)	315 (1.13)	357 (−1.02)	389 (1.48)
	673 (5.44)	745 (16.8)	457 (−1.70)	498 (0.26)	663 (2.63)
			723 (4.52)	755 (−8.33)	

[a] λ/nm (10^{-4} ϵ/dm^3 mol^{-1} cm^{-1}). [b] λ/nm (10^{-5} $[\theta]_M$/deg dm^3 mol^{-1}cm^{-1} T^{-1}). [c] sh denotes shoulder.

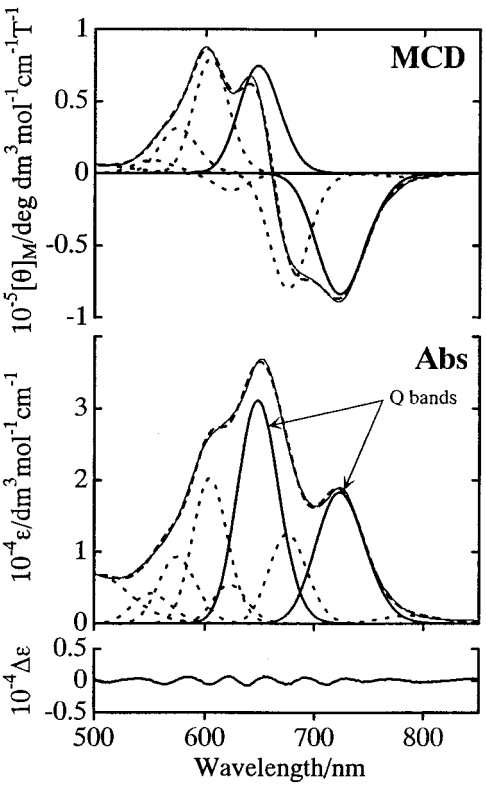

Figure 6. Simultaneous band deconvolution analysis of the Q absorption and MCD bands of CoAnAP. Split Q_{00}-bands are shown by bold solid lines, while the experimental curves are shown as thin solid lines. The bottom part shows the deviation of the simulated absorption spectrum from the experimental absorption spectrum.

It is generally known that oxidized species aggregate more easily than neutral species,[33] and since it takes time for aggregation to occur, the peak that becomes more prominent at higher scan rates or at lower sample concentrations is due to the nonaggregated monomer species. Interestingly, oxidation of aggregates always occurs at less positive potentials than that of nonaggregated species.[34]

Voltammograms of cobalt TAPs, Pc's, and naphthalocyanines generally differ from those of the zinc, copper, and nickel complexes, in showing redox couples due to cobalt oxidation and reduction. In this study, the assignment of the couples is based on the previous data[29] on redox couples of TAPs and Pc's, as well as spectroelectrochemical data to be treated in a later section. As a result, the first and second reductions of all the compounds in *o*-DCB were assigned to the $Co^{II/I}$ and the first ligand reduction ($L^{-2/-3}$) couples,[35] respectively, while the first and second oxidations were assigned to the ligand first oxidation and $Co^{III/II}$ couples, respectively, except in the case of CoTAP. The assignment of the two oxidation couples of CoTAP could not be performed, even by the spectroelectrochemical method, due to the low solubility. Accordingly, the result of highly soluble tetra-*tert*-butylated CoTAP[36] in *o*-DCB was employed, and then the first oxidation was tentatively assigned to the $Co^{III/II}$ couple and the second to the ligand first oxidation. These assignments match well with the series of data, since all redox couples of the monosubstituted ABBB type (left-hand side in Figure 8) appear at more positive potentials than those of the corresponding adjacently disubstituted AABB type species (right-hand side in Figure 8). This means that the fused aromatics function as electron-releasing groups. Accordingly, the first ligand reduction of AABB type species is more difficult than that of the ABBB type species, but conversely the first ligand oxidation of the former is easier than that of the latter because of the higher electron density in the central TAP moiety of the former. The first ligand reduction of CoTAP occurs, for

(33) Fuhrhop, J. H.; Wasser, P.; Riesner, D.; Mauzeral, D. *J. Am. Chem. Soc.* **1972**, *94*, 7996. Song, H.; Reed, C. A.; Scheidt, W. R. *J. Am. Chem. Soc.* **1989**, *111*, 6865. Schulz, C. Z.; Song, H.; Mislanker, A.; Orosz, R. D.; Reed, C. A.; Debrunner, P. G.; Scheidt, W. R. *Inorg. Chem.* **1997**, *36*, 406.

(34) Kadish, K. M. *Recent Prog. Inorg. Chem.* **1986**, *34*, 435. Kobayashi, N.; Miwa, H.; Isago, H.; Tomura, T. *Inorg. Chem.* **1999**, *38*, 479.

(35) The standard oxidation potential of the Pc and TAP anion is represented by Pc(−2) and TAP(−2). Thus, if L indicates a general ligand, the first oxidized and first reduced species will be represented by L(−1) and L(−3), respectively.

(36) Kobayashi, N.; Nakajima, S.; Osa, T. *Chem. Lett.* **1992**, 2415.

Table 2. Band Fitting Parameters[a] of the Q-Band Used for Deconvolution Analysis

compd	ν/cm^{-1}	λ/nm^{-1}	ϵ_{max}	$\Delta\nu$/cm^{-1}	$\langle\epsilon\rangle_0$	D_0	f	MCD int.[b]	type	$\langle\epsilon_M\rangle_n$	$10^3A_1(B_0)$	$10^3B_0/D_0$	A_1/D_0
CoTAP	16329	612	39134	970	2474	7.58	0.17	−144009	*A*	1.92×10^3	12.6×10^3		1.66
								−50010	*B*	−0.96	−6.30	−0.83	
CoBzAP	15265	655	36615	1047	2674	8.19	0.18	−262869	*B*	−5.81	−38.1	−4.65	
	16029	624	41611	1020	2820	8.63	0.20	129930	*B*	2.67	17.5	2.02	
CoNpAP	14499	690	30728	991	2235	6.84	0.14	−160405	*B*	−3.55	−23.3	−3.40	
	15901	629	37894	1083	2748	8.41	0.19	160975	*B*	3.55	23.3	2.77	
CoAnAP	13811	724	18305	1004	1418	4.34	0.08	−83593	*B*	−1.96	−12.9	−2.97	
	15419	649	31060	1052	2256	6.91	0.15	74503	*B*	1.64	10.8	1.56	
$CoBz_2AP$	14936	670	74657	937	4986	15.3	0.32	−269354	*A*	3.67×10^3	24.1×10^3		1.58
								−121379	*B*	−2.46	−16.1	−1.05	
$CoNp_2AP$	14102	709	53496	1036	4182	12.8	0.25	−211222	*A*	3.76×10^3	24.7×10^3		1.93
								−100770	*B*	−2.39	−15.7	−1.23	
$CoAn_2AP$	13409	746	73298	814	4739	14.5	0.27	−262892	*A*	3.02×10^3	19.8×10^3		1.37
								−193741	*B*	−3.79	−24.9	−1.72	

[a] D (dipole strength) $= \langle\epsilon\rangle_0/326.6$. f is the oscillator strength. $\langle\epsilon_M\rangle_0$ ($n = 0$) and $\langle\epsilon_M\rangle_1$ ($n = 1$) are the zeroth and first moments of the MCD *B*- and *A*-terms, respectively. $A_1 = \langle\epsilon_M\rangle_1/152.5$ and $B_0 = \langle\epsilon_M\rangle_0/152.5$. [b] MCD intensity is based on molar ellipticity per tesla.

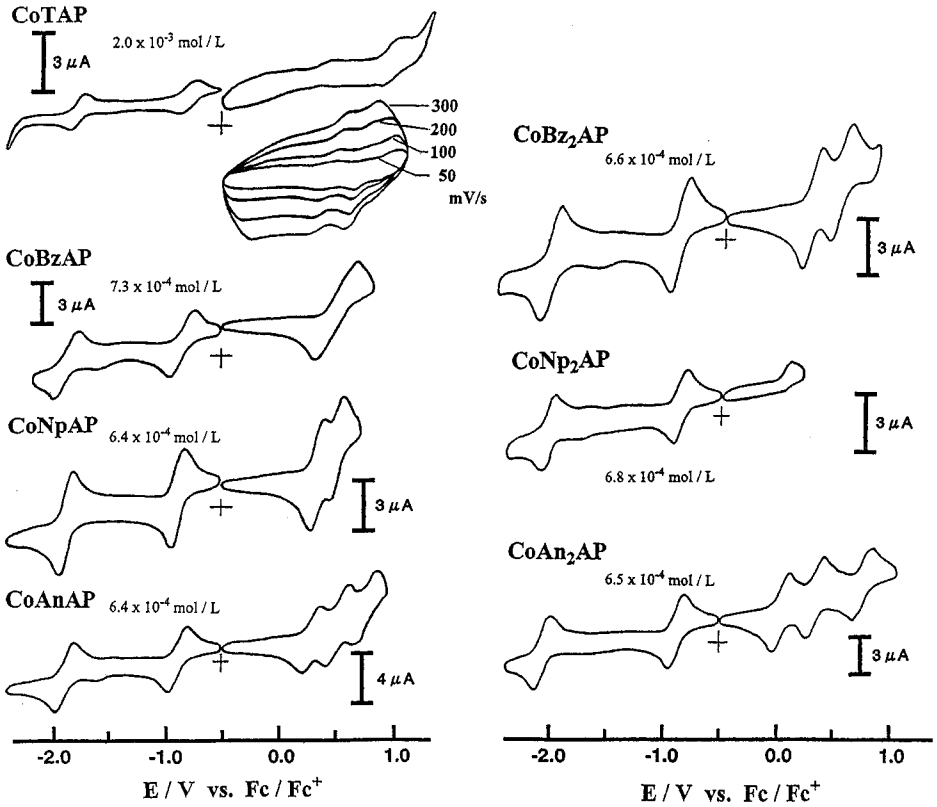

Figure 7. Cyclic voltammograms of the cobalt complexes in this study in *o*-DCB containing 0.1 mol/L TBAP.

the same reason, at a slightly more positive potential than those of ABBB and AABB type species. Plots in Figure 8 also indicate that the first ligand reduction potentials among the ABBB type species do not change much from species to species. This is true also for AABB type species, although the potential is slightly more negative than that of the ABBB type species, indicating that the LUMO level does not sensitively change. However, it is seen that the change in the first ligand oxidation potential is more marked than that in the first ligand reduction potentials. In addition, since the oxidation becomes easier with increasing molecular size, it is concluded that the HOMO destabilizes significantly with enlargement of the π system. This is consistent with the hitherto predicted[17a−c] and accumulated[37] data and is reproduced by MO calculations described in the following section. The potential difference between the first ligand oxidation of CoTAP and CoBzAP or $CoBz_2AP$ may still appear large; however, there is a reason for this. The cobalt center is first oxidized to Co^{III}, and this positive charge delocalizes to some extent into the TAP ligand, thereby making oxidation of the ligand more difficult.[38] The first ligand oxidations of CoBzAP and $Co^{III/II}$ coincidentally occur experimentally at the same potential, due to the positive shift of the first ligand oxidation potential.

(iv) Molecular Orbital Calculations. To enhance our understanding of the electronic spectra, we have performed MO

(37) Kobayashi, N.; Nakajima, S.; Osa, T. *Inorg. Chim. Acta* **1993**, *210*, 131.

(38) A similar reason has been adopted to explain the relatively negative first reduction potentials of cobalt Pc derivatives compared with those in nickel, copper, and zinc derivatives.[29] In this case, however, the first ligand reduction of Pc appears after the cobalt$^{II/I}$ couple. Accordingly, partial negative charge from the reduced cobalt delocalizes to the ligand, thereby making the first ligand reduction more negative or difficult.

Table 3. Redox Potential Data (vs Fc^+/Fc) in *o*-DCB Containing 0.1 M TBAP[a]

couple	$E_{1/2}$/V	ΔE_p/mV	couple	$E_{1/2}$/V	ΔE_p/mV
CoTAP					
$Co^{III}L(-1)/Co^{III}L(-2)$	0.94	130			
$Co^{III}L(-2)/Co^{II}L(-2)$	0.68				
$Co^{II}L(-2)/Co^{I}L(-2)$	−0.81	120			
$Co^{I}L(-2)/Co^{I}(-3)$	−1.77	110			
CoBzAP			$CoBz_2AP$		
$Co^{III}L(-1)/Co^{III}L(-2)$	0.48	350	$Co^{III}L(-1)/Co^{II}L(-1)$	0.50	170
$Co^{III}L(-2)/Co^{II}L(-2)$	0.48	350	$Co^{II}L(-1)/Co^{II}L(-2)$	0.25	165
$Co^{II}L(-2)/Co^{I}L(-2)$	−0.85	210	$Co^{II}L(-2)/Co^{I}L(-2)$	−0.87	150
$Co^{I}L(-2)/Co^{I}(-3)$	−1.85	210	$Co^{I}L(-2)/Co^{I}(-3)$	−1.97	150
CoNpAP			$CoNp_2AP$		
$Co^{III}L(-1)/Co^{II}L(-1)$	0.48	120	$Co^{III}L(-1)/Co^{II}L(-1)$	not obsd	
$Co^{II}L(-1)/Co^{II}L(-2)$	0.32	120	$Co^{II}L(-1)/Co^{II}L(-2)$[b]	0.09	
$Co^{II}L(-2)/Co^{I}L(-2)$	−0.86	120	$Co^{II}L(-2)/Co^{I}L(-2)$	−0.86	110
$Co^{I}L(-2)/Co^{I}(-3)$	−1.83	105	$Co^{I}L(-2)/Co^{I}(-3)$	−1.96	110
CoAnAP			$CoAn_2AP$		
$Co^{III}L(0)/Co^{III}L(-1)$	0.75	180	$Co^{III}L(0)/Co^{III}L(-1)$	0.70	160
$Co^{III}L(-1)/Co^{II}L(-1)$	0.50	200	$Co^{III}L(-1)/Co^{II}L(-1)$	0.31	135
$Co^{II}L(-1)/Co^{II}L(-2)$	0.28	155	$Co^{II}L(-1)/Co^{II}L(-2)$	0.01	140
$Co^{II}L(-2)/Co^{I}L(-2)$	−0.86	160	$Co^{II}L(-2)/Co^{I}L(-2)$	−0.88	130
$Co^{I}L(-2)/Co^{I}(-3)$	−1.81	170	$Co^{I}L(-2)/Co^{I}(-3)$	−2.01	130
NiAnAP			$NiAn_2AP$		
L(−1)/L(−2)	0.46	140	L(0)/L(−1)	0.57	130
L(−2)/L(−3)	−1.24	120	L(−1)/L(−2)	0.20	130
L(−3)/L(−4)	−1.56	115	L(−2)/L(−3)	−1.45	140
			L(−3)/L(−4)	−1.81	140

[a] ΔE_p is the potential difference between cathodic and anodic peak potentials at a sweep rate of 30 mV/s. L, ligand. [b] Data from differential pulse voltammogram.

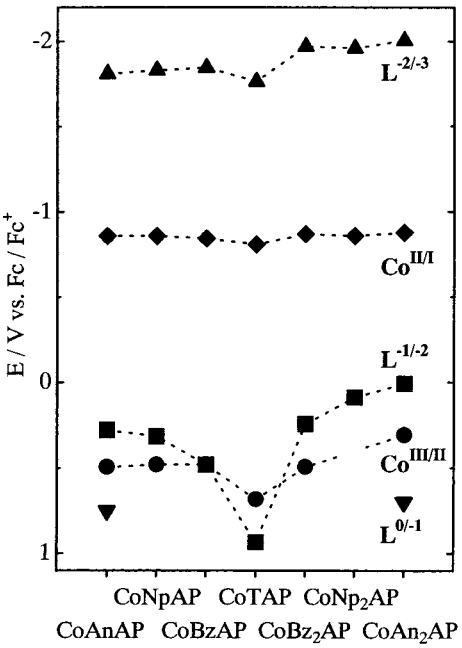

Figure 8. Electrochemically obtained redox data of cobalt derivatives in *o*-DCB. $L^{-2/-3}$ and $L^{-1/-2}$ correspond to the ligand first reduction and oxidation, respectively.

calculations within the framework of the PPP approximation and ZINDO/S Hamiltonian. The ZINDO/S method is more recent than the PPP method and has parameters for some metals, but the computation time is long, and the calculations generally underestimate transition energies.[39] The PPP method has been known for a long time and needs no parameters for the metals.

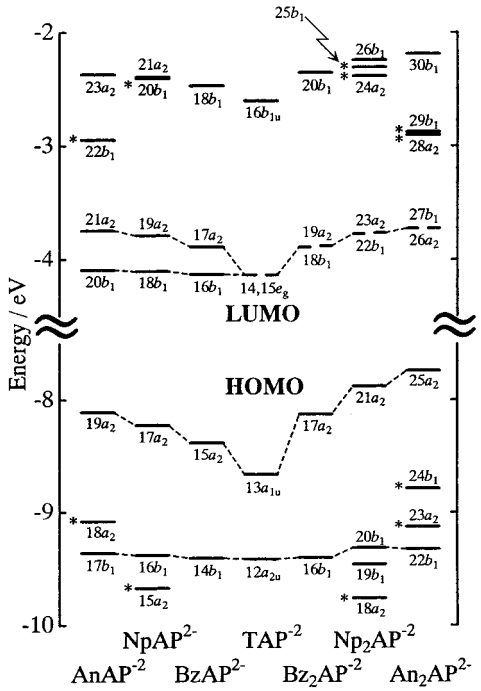

Figure 9. Partial energy diagram for the (pyrrole proton-) deprotonated ABBB and AABB type species. Orbitals marked by ∗ are either naphthalene- or anthracene-centered orbitals. See the text concerning orbital $20b_1$ of Np_2AP^{2-}.

It requires short computation times, and a great amount of data have been accumulated in the past (calculations on macrocycles slightly overestimate transition energies).[14b] The results described here are mostly based on the PPP method, unless otherwise noted.

Partial MO energy diagrams for four frontier orbitals of (pyrrole proton-) deprotonated ABBB and AABB type species are shown in Figures 9 and 10, respectively, with calculated transition energies, oscillator strengths (*f*), and configurations summarized in Table 4. As described in Figure 9, all the HOMOs and LUMOs+1 belong to the a_2, while the LUMOs belong to the b_1 irreducible representations, respectively. In the same figure, the orbitals marked by ∗ represent the naphthalene- or anthracene-centered orbitals. These orbitals, however, barely contribute to the Q-band, as seen in the configurations in Table 4. Accordingly, in considering a four-orbital model[40,41] in which the optical spectrum can be interpreted in terms of two HOMOs and LUMOs, these orbitals were not taken into account. In the case of Np_2AP, the $20b_1$ orbital might be considered to be, from the size of the coefficients, a naphthalene-centered orbital, but it was taken as the HOMO−1 since it had fair coefficients over the central TAP moiety, and this orbital contributed substantially to the Q-band (Table 4). Hence, we can consider that all the HOMOs−1 belong to b_1 symmetry. In the C_{2v} point group, the *z*-axis is an in-plane axis, and therefore all one-electron transitions become allowed transitions, at least in one direction.

(39) Ishii, K.; Kobayashi, N.; Matsuo, T.; Tanaka, M.; Sekiguchi, A. *J. Am. Chem. Soc.* **2001**, *123*, 5356. Mack, J.; Kobayashi, N.; Leznoff, C. C.; Stillman, M. J. *Inorg. Chem.* **1997**, *36*, 5624.
(40) Gouterman, M. In *The Porphyrins*; Dolphin, D., Ed.; Academic Press: New York, 1978; Vol. III, Part A, Chapter 1. Gouterman, M. *J. Chem. Phys.* **1959**, *30*, 1139.
(41) To our knowledge, the spectra of porphyrin or Pc derivatives can be explained by Gouterman's four-orbital model except for one case, which was explained by a five-orbital model including two LUMOs and three HOMOs (Kobayashi, N.; Sasaki, N.; Konami, H. *Inorg. Chem.* **1997**, *36*, 5674).

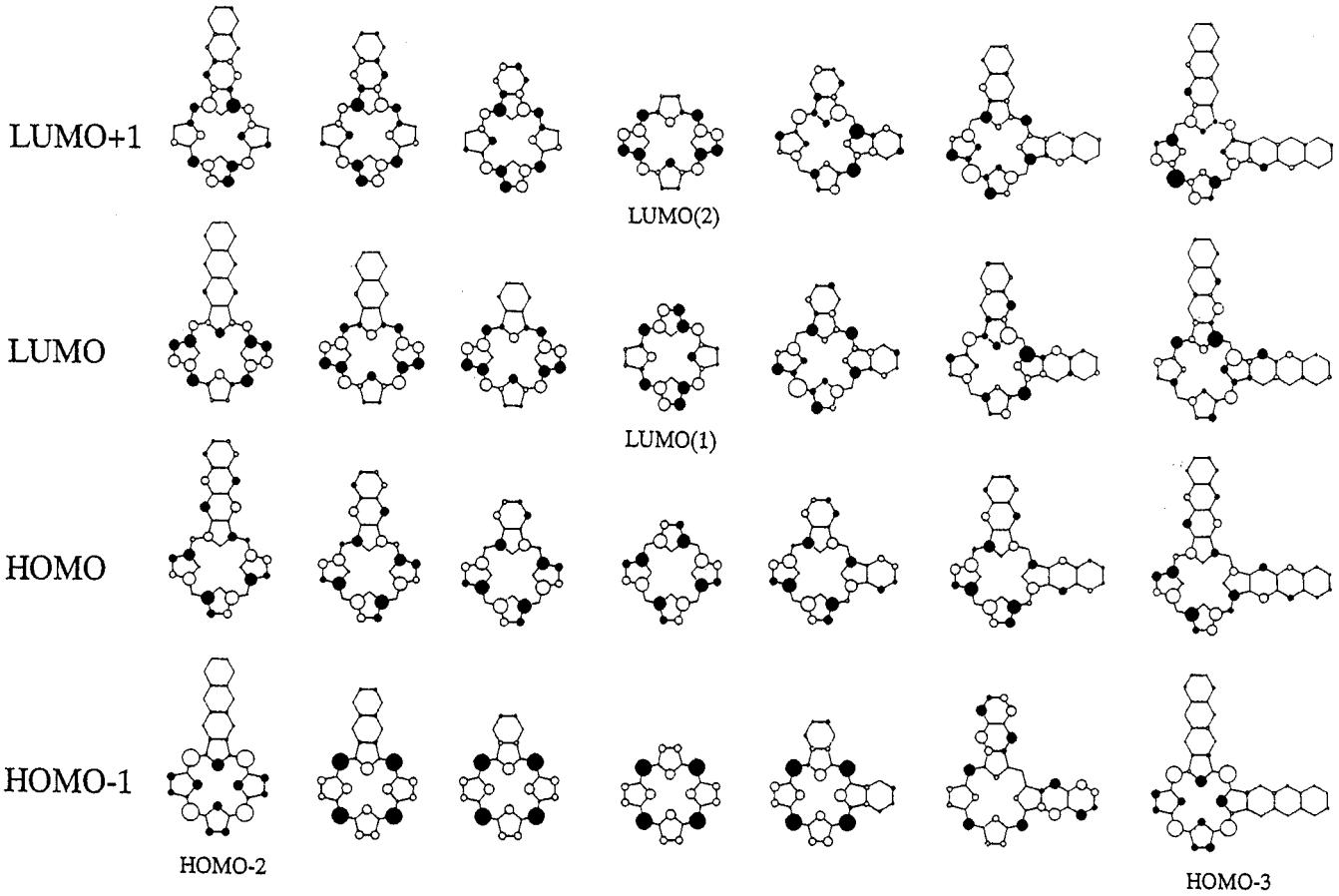

Figure 10. Four frontier orbitals of the (pyrrole proton-) deprotonated ABBB and AABB type species. Note that LUMO(1) and LUMO(2) of TAP^{2-} are degenerate, while the anthracene-centered orbitals in $AnAP^{2-}$ (i.e., HOMO−1), An_2AP^{2-} (HOMO−1), and An_2AP^{2-} (HOMO-2) are excluded, since their contribution to the Q-band is small.

In the preceding section, it was found experimentally that the LUMO energy remained almost constant while the HOMO energy destabilized with increasing size of the fused aromatics. As seen in Figure 9, this is almost perfectly reproduced, confirming the reliability of the calculations (note in particular that the potential change of the $L^{-2/-3}$ couple in Figure 8, i.e., the first ligand reduction, correlates perfectly with the change of the LUMO energies in Figure 9, while the potential change of the $L^{-1/-2}$ couple in Figure 8, i.e., the first ligand oxidation, correlates nicely with the change of the HOMO energies in Figure 9). Although this phenomenon concerning the HOMO and LUMO levels on ring-expansion has been noted several times in the past,[17a−c,37] no one has succeeded in explaining it. Indeed, this is a strange phenomenon, taking into account that the energies of both the HOMO and LUMO levels of normal hydrocarbons change to an almost comparable extent with changing size of the π system.[42] The resolution of this question is given reasonably, however, for the first time from the careful discernment of the MOs drawn in Figure 10. As typically seen for a series of ABBB type species, the HOMOs spread over the whole molecule, while the LUMOs are localized in the central TAP moiety and have only small coefficients over the fused aromatics. Accordingly, the LUMO energy is essentially fixed, irrespective of the size of the π system, while the HOMO energy destabilizes with increasing molecular size. Similar localization is seen for the HOMO−1 levels (Figure 10), and indeed the energy does not change sensitively with size (Figure 9). The LUMO+1 levels, on the other hand, have coefficients over the whole molecule, and therefore they destabilize with increasing molecular size (Figure 9), as for the HOMO. In the cases of the disubstituted AABB type species, the above trend is less obvious, but still the coefficients over the fused aromatic moiety are larger for the HOMO than the LUMO levels, so that the change of the energy level is larger for the HOMO levels than for the LUMO levels. In addition, specifically for the AABB type species, the increase in magnitude of the coefficients of the LUMO and LUMO+1 levels is very similar over each molecule, so that the energy shifts of the LUMO and LUMO+1 levels on ring expansion are very similar and thus remain almost degenerate. Thus, we can reasonably explain the shift of MO levels on the basis of the magnitude of their coefficients. The explanation and interpretation used here for the behavior of the HOMO and LUMO levels based on the coefficient of their molecular orbitals appear valid when applied to other macrocyclic systems.

Figure 11 shows the calculated absorption spectra. For monosubstituted ABBB type species, split Q-bands are calculated between 577 and 637 nm, shorter than experimentally observed (624−724 nm). This is due, in part, to the large substituent effect of the eight phenyl groups (estimated to be

(42) For example, in our calculations using the ZINDO/S Hamiltonian on benzene, naphthalene, and anthracene, the energy of the HOMOs changed from −9.825 to −7.025, and further to −5.514 eV, while that of the LUMOs changed from 8.064 to 5.963, and further to 4.656 eV in the order of the above compounds.

Table 4. Calculated Transition Energies, Oscillator Strength (*f*), and Configurations for Deprotonated TAP Derivatives[a]

energy/eV	/nm	*f*	configurations[b]			energy/eV	/nm	*f*	configurations[b]		
			TAP^{2-}								
2.10	589	0.14	13→15 (67%)	12→14 (33%)							
2.10	589	0.14	13→14 (67%)	12→15 (33%)							
3.22	385	0.30	8→15 (37%)	11→15 (33%)	12→15 (10%)						
			13→14 (10%)								
3.22	385	0.30	8→14 (37%)	11→14 (33%)	12→14 (10%)						
			13→15 (10%)								
3.85	322	1.83	12→14 (31%)	11→14 (29%)	13→15 (13%)						
			12→15 (11%)	11→15 (10%)							
3.85	322	1.83	12→15 (31%)	11→15 (29%)	13→14 (13%)						
			12→14 (11%)	11→14 (10%)							
3.98	311	1.18	8→15 (38%)	8→14 (19%)	11→15 (15%)						
			12→15 (10%)								
3.98	311	1.18	8→14 (38%)	8→15 (19%)	11→14 (15%)						
			12→14 (10%)								
			$BzAP^{2-}$						Bz_2AP^{2-}		
2.04	609	0.30	15→16 (76%)	14→17 (23%)		2.04	609	0.41	17→18 (78%)	16→19 (22%)	
2.15	577	0.21	15→17 (69%)	14→16 (30%)		2.08	595	0.42	17→19 (79%)	16→18 (20%)	
3.17	391	0.41	11→16 (66%)	14→16 (12%)	15→17 (11%)	3.31	374	0.35	14→18 (50%)	15→19 (18%)	16→18 (16%)
3.38	367	0.29	13→17 (67%)	14→17 (14%)		3.32	373	0.37	15→18 (52%)	14→19 (20%)	16→19 (13%)
3.73	332	1.56	13→16 (42%)	14→16 (34%)	15→17 (12%)	3.56	348	0.14	17→20 (85%)		
3.74	332	0.81	10→17 (40%)	14→17 (27%)	13→17 (17%)	3.65	340	1.07	16→19 (31%)	15→18 (17%)	11→19 (16%)
3.82	325	1.39	13→16 (51%)	14→16 (21%)	11→16 (11%)				17→20 (11%)	17→18 (10%)	
4.00	310	1.37	10→17 (36%)	14→17 (31%)	11→17 (13%)	3.66	339	1.22	16→18 (34%)	12→19 (22%)	14→18 (16%)
									11→18 (12%)		
						3.88	319	0.69	11→19 (35%)	12→18 (16%)	14→19 (14%)
									16→19 (13%)	15→18 (11%)	
						3.89	319	1.33	12→19 (38%)	16→18 (28%)	11→18 (13%)
						4.00	310	0.77	14→19 (56%)	15→18 (13%)	
			$NpAP^{2-}$						Np_2AP^{2-}		
1.98	625	0.38	17→18 (80%)	16→19 (20%)		1.95	634	0.62	21→22 (82%)	20→23 (13%)	
2.15	577	0.33	17→19 (72%)	16→18 (27%)		2.06	603	0.61	21→23 (84%)	20→22 (11%)	
3.18	390	1.21	12→18 (44%)	16→18 (27%)	17→19 (15%)	3.26	381	0.96	19→23 (46%)	17→22 (15%)	21→26 (13%)
3.43	362	0.28	14→19 (66%)	16→19 (17%)		3.29	377	0.78	20→22 (36%)	16→22 (36%)	17→23 (10%)
3.45	359	1.02	12→18 (34%)	15→19 (25%)	17→20 (17%)	3.49	355	0.75	16→22 (32%)	20→22 (25%)	18→23 (22%)
			16→18 (13%)			3.56	348	0.15	21→26 (73%)	19→23 (20%)	
3.62	342	0.14	15→18 (70%)			3.62	343	0.63	21→25 (46%)	20→23 (22%)	17→22 (14%)
3.66	339	0.23	17→20 (60%)	14→18 (26%)		3.72	333	0.38	21→25 (43%)	20→23 (35%)	17→22 (11%)
3.75	330	0.11	14→18 (71%)	17→20 (21%)		3.76	330	0.71	19→22 (64%)		
3.93	315	1.95	16→19 (49%)	15→18 (22%)		3.99	311	0.41	18→23 (41%)	20→22 (17%)	
4.06	305	0.73	15→19 (57%)	16→18 (25%)		4.06	306	0.12	17→23 (65%)	18→23 (11%)	
						4.07	305	0.69	16→23 (40%)	18→22 (23%)	
			$AnAP^{2-}$						An_2AP^{2-}		
1.95	637	0.39	19→20 (80%)	17→21 (18%)		1.91	649	0.76	25→27 (83%)	22→26 (13%)	
2.14	579	0.41	19→21 (71%)	17→20 (25%)		2.02	614	0.73	25→26 (85%)	22→27 (12%)	
3.04	408	1.29	17→20 (27%)	13→20 (21%)	19→21 (18%)	2.95	420	0.40	24→26 (65%)	22→26 (11%)	
			18→21 (17%)			3.08	402	0.44	25→29 (74%)		
3.30	376	0.20	18→21 (35%)	13→20 (23%)	15→20 (23%)	3.14	394	0.90	24→27 (43%)	23→26 (18%)	22→27 (15%)
3.45	360	0.20	16→21 (66%)	18→20 (10%)	17→21 (10%)	3.29	377	0.27	21→27 (34%)	24→26 (14%)	22→26 (13%)
3.62	342	0.10	19→23 (72%)	16→20 (16%)		3.43	362	0.25	24→27 (39%)	23→26 (26%)	22→27 (13%)
3.77	329	2.15	17→20 (30%)	16→20 (21%)	18→21 (15%)	3.54	351	0.22	25→30 (44%)	23→27 (23%)	21→27 (13%)
			13→20 (12%)			3.66	339	0.54	22→26 (30%)	24→28 (19%)	21→27 (13%)
3.84	323	0.68	17→21 (38%)	18→22 (31%)	16→21 (15%)	3.69	336	0.51	22→27 (35%)	24→29 (21%)	23→28 (12%)
4.00	310	1.42	18→22 (51%)	17→21 (18%)					20→27 (10%)		
4.30	289	0.15	15→21 (51%)	13→21 (42%)		3.86	321	1.69	24→29 (28%)	23→28 (16%)	23→26 (14%)
									22→27 (10%)		
						3.87	320	0.95	23→27 (25%)	24→28 (25%)	23→29 (21%)
						4.04	307	0.47	20→26 (71%)	21→27 (12%)	

[a] Excited states with less than 4.1 eV and $f > 0.10$ are shown. [b] Orbital numbers 13, 15, 17, 19, 17, 21, and 25 are HOMOs of TAP^{2-}, $BzAP^{2-}$, $NpAP^{2-}$, $AnAP^{2-}$, Bz_2AP^{2-}, Np_2AP^{2-}, and An_2AP^{2-}, respectively. In $NpAP^{2-}$ and Np_2Ap^{2-}, the MOs numbered 15, 20 and 18, 24, and 25 are naphthalene-centered orbitals in the above compounds order. Similarly, in $AnAP^{2-}$ and An_2AP^{2-}, MOs 18, 22 and 23, 24, 28, and 29 are anthracene-centered orbitals, respectively.

ca. 1260−1300 cm^{-1})[19b,33,43] Of the split Q-band, the transitions at shorter wavelength are estimated at 577, 577, and 579 nm without much variation, in the order of $BzAP^{2-}$, $NpAP^{2-}$, and $AnAP^{2-}$, respectively, while those at longer wavelengths are calculated at 609, 625, and 637 nm, in the above order, reproducing the trend observed experimentally (Figure 4A). The calculated splitting energies are 910, 1330, and 1570 cm^{-1}, also showing close resemblance to experiment (ca. 760, 1400, and 1610 cm^{-1}, respectively). Experimentally, the relative intensity of the longer wavelength component to the shorter wavelength

(43) Luk'yanets, E. A. *Electronic Spectra of Phthalocyanines and Related Compounds*; NIOPIK: Moscow, 1989.

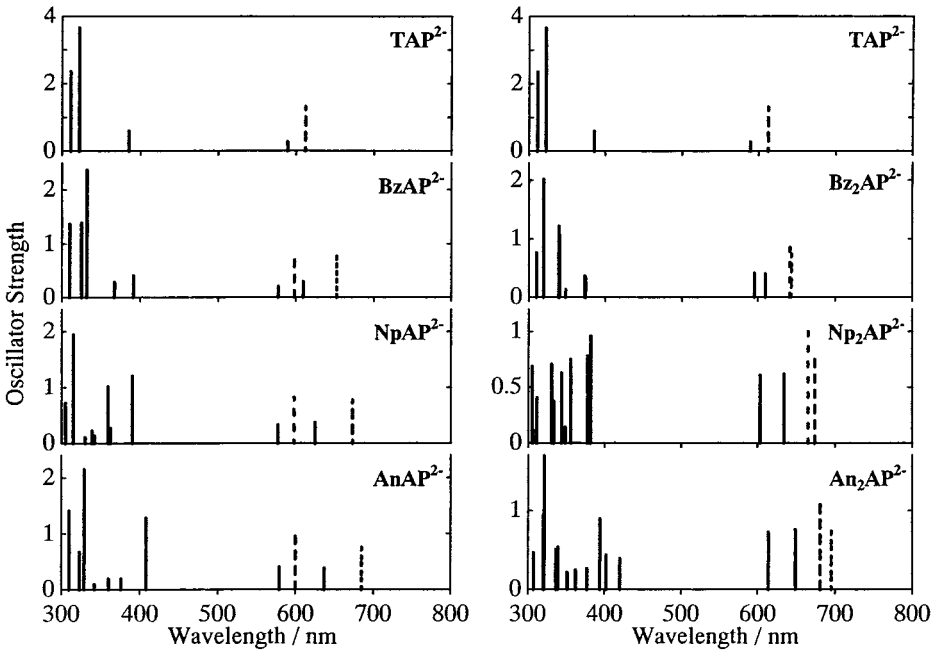

Figure 11. Calculated, within the framework of the PPP approximation, absorption spectra for the (pyrrole proton-) deprotonated species. Broken lines indicate the Q-band obtained using the ZINDO/S Hamiltonian.

component was found to decrease from 0.90 to 0.74 and further to 0.53 (Table 2) on going from CoBzAP to CoNpAP and further to CoAnAP. Although this trend is reproduced, the reproducibility of the absolute value is not good (1.43, 1.15, and 0.95, respectively). For all ABBB type species, more than 90% of the Q-band is composed of the four one-electron transitions from the HOMO and HOMO−1 to LUMO and LUMO+1 (Table 4). The Q-bands to the shorter wavelength are composed of the HOMO→LUMO+1 and the HOMO−1→LUMO transitions. Since neither the HOMO−1 nor LUMO shows significant energy variation on ring expansion, their energy gaps are similar, being 5.28, 5.28, and 5.27 eV for $BzAP^{2-}$, $NpAP^{2-}$, and $AnAP^{2-}$, respectively. On the other hand, both the HOMO and LUMO+1 energy levels increase at a similar rate, so that their energy gap shows little variation on ring expansion, i.e., 4.50, 4.44, and 4.37 eV in the above order. Accordingly, the one-electron excitation energy constituting the shorter wavelength Q-band remains almost constant, irrespective of the size of the ligand. The Q-bands to longer wavelength are composed of the HOMO→LUMO and the HOMO−1→LUMO+1 transitions. The energy gap between the HOMO and LUMO decreases, while that between the HOMO−1 and LUMO+1 increases with increasing size of the π system. The magnitude of the contribution of a certain one-electron transition to an observed transition can be estimated by the magnitude of the product of the electronic transition moment and the coefficient of the one-electron transition in the wave functions of the excited states. For the HOMO→LUMO transition, the values were 2.22 for both BzAP and NpAP and 2.12 for AnAP, respectively. By calculating similarly for the HOMO−1→LUMO+1 transition, values of 0.92, 0.81, and 0.76 were obtained in the order of the above compounds. Accordingly, the contribution of the HOMO→LUMO transition to the longer wavelength Q-band is larger. Hence, it is concluded that the Q-band-shift to longer wavelength is a result of a reduction of energy between the HOMO and LUMO.

From the configuration in Table 4, the Soret bands of BzAP and NpAP may correspond to the bands at 332 and 367 nm, and 330 and 362 nm, respectively. However, since the Soret band spectra are composed of a superimposition of broad bands (Figure 4A), comparison with the calculation results is difficult. In the case of $AnAP^{2-}$, transitions arising from the anthracene moiety overlap, so that it is even more difficult to determine which transition corresponds to the Soret band.

Next, we consider the spectra of adjacently disubstituted AABB type species. As shown in Table 4, the estimated splitting of the Q-band is smaller than that in the ABBB type species (390, 810, and 880 cm^{-1} for Bz_2AP^{2-}, Np_2AP^{2-}, and An_2AP^{2-}, respectively), while the intensities of the two bands are very close, i.e., 0.42 and 0.41, 0.61 and 0.62, and 0.73 and 0.76, respectively, in order of the above compounds. In Figure 5, the Q_{00}-band appeared degenerate and could be fitted using a single Gaussian curve, while the Q MCD band was fitted as a Faraday *A*-term. However, the calculation results here indicate that the Q-bands split slightly, and therefore that the Q state is nearly degenerate (according to the results on the basis of ZINDO/S Hamiltonian, the above values (390, 810, and 880 cm^{-1}) were improved to ca. 50, 200, and 300 cm^{-1}, respectively (see also broken lines in Figure 11)).[44] However, in the cases of AABB type species, the energies of the LUMO and LUMO+1 are very similar, so that energies composed of the HOMO→LUMO+1 and the HOMO−1→LUMO transitions and the HOMO→LUMO and the HOMO−1→LUMO+1 transitions become nearly equal, giving rise to the *pseudo*-degeneracy of the Q-band.[45] The

(44) From the symmetry-adapted perturbation (SAP) method,[17a,b] only a shift of the Q-band is expected without detectable energy splitting. However, this is understood within the precision of the first-order perturbation (note that the SAP is a first-order perturbation). A Q-band split predicted by the MO calculations is not surprising since the PPP calculation was based on the actual C_{2v} symmetry and included much higher perturbation terms than the SAP method. Since the results of MO calculations showed splitting of the Q-band, the dispersion type Q-band MCD in Figure 5B is actually a *pseudo* Faraday *A*-term, which is produced by the superimposition of closely lying, interacting Faraday *B*-terms.[24]

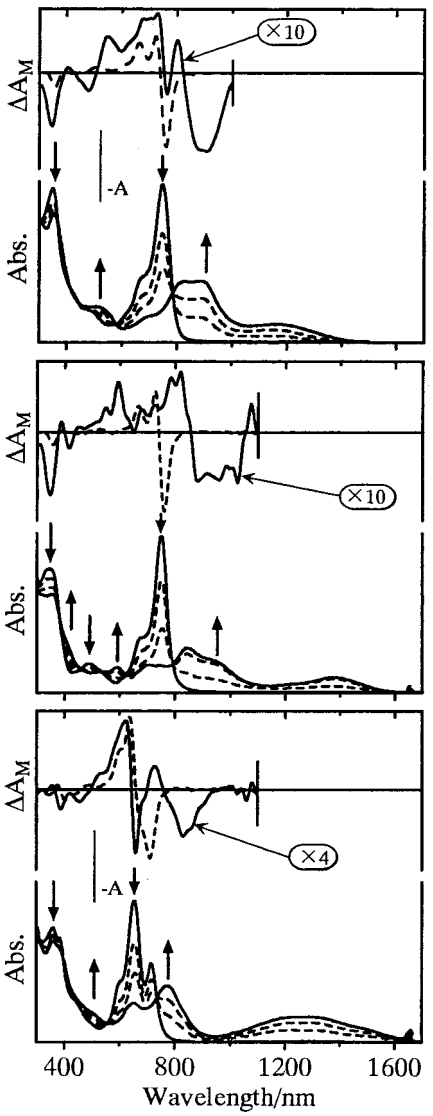

Figure 12. Development of the electronic absorption and MCD spectra with time during the oxidation of $CoAn_2AP$ (top) at 0.70, $NiAn_2AP$ (middle) at 0.90, and CoAnAP (bottom) at 0.90 V vs Ag/AgCl in *o*-DCB (0.3 M TBAP) to ring-oxidized cation radicals. The directions of spectroscopic changes are shown by the bold arrows. The MCD spectrum of the starting neutral species is shown as a broken line, and that of the electrolyzed species is shown as a solid line. Note the encircled magnification factor for the MCD spectrum of oxidized species.

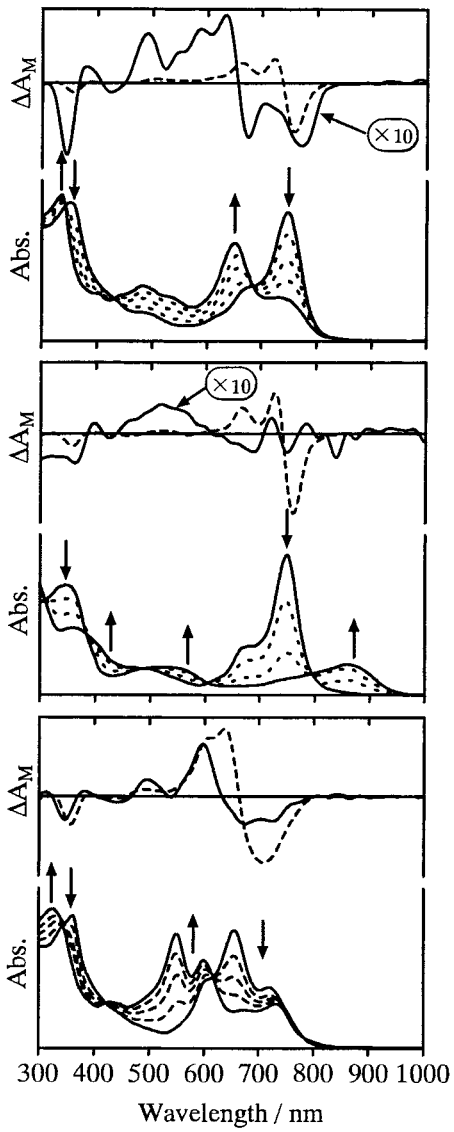

Figure 13. Development of the electronic absorption and MCD spectra with time during the reduction of $CoAn_2AP$ (top) at −1.00, $NiAn_2AP$ (middle) at −1.30, and CoAnAP (bottom) at −1.00 V vs Ag/AgCl in *o*-DCB (0.3 M TBAP) to Co^I species ($CoAn_2AP$ and CoAnAP) or a ring-reduced anion radical ($NiAn_2AP$). The directions of spectroscopic changes are shown by the bold arrows. The MCD spectrum of the starting neutral species is shown as a broken line, and that of the electrolyzed species is shown as a solid line. Note the encircled magnification factor for the MCD spectrum of reduced species.

destabilization of the HOMO on ring expansion is the cause of the red shift of the Q-band.

Thus, as described above, the characteristics of the Q-band of both ABBB and AABB type species can be rationalized in the level of molecular orbitals.

(v) Spectroelectrochemistry. Spectroelectrochemistry has been performed in order to facilitate the assignment of some of the redox couples and to illustrate the characteristics of the spectra of electrolyzed species of low symmetrical TAPs. Figures 12 and 13 show the development of the spectra during the first oxidation and reduction, respectively. In general, nickel TAPs and Pc's do not show couples due to nickel within the potentials applied. Accordingly, the spectra of nickel species can be used as exemplary data for the ring-oxidized or -reduced species. During the course of the oxidation of $NiAn_2AP$ (Figure 12, middle), the Q-band lost intensity, and instead, broad bands appeared at the longer wavelength side, at ca. 800−1050 and 1200−1500 nm. MCD showed a broad negative band corresponding to the 800−1050 nm band (positive Faraday *B*-term). These broad bands are produced by dimerization of cationic radical species.[46] The Soret band shifted to the red and lost intensity slightly on oxidation. The spectroscopic change of $CoAn_2AP$ on the first oxidation (Figure 12, top) is similar to that seen for $NiAn_2AP$, indicating that the oxidation is ligand-centered. However, a different behavior was observed in the

(45) Ballhausen, C. J. *Introduction to Ligand Field Theory*; McGraw-Hill: New York, 1962.

(46) (a) Stillman, M. J. In *Phthalocyanines: Properties and Applications*; Leznoff, C. C., Lever, A. B. P., Eds.; VCH: New York, 1993; Vol. 3, Chapter 5. (b) Nevin, W. A.; Liu, W.; Greenberg, S.; Hempstead, M. R.; Marcuccio, S. M.; Melnik, M.; Leznoff, C. C.; Lever, A. B. P. *Inorg. Chem.* **1987**, *26*, 891.

region between the Soret band and the Q-band, where a small band developed with electrolysis and an associated negative Faraday *A* MCD-term was observed. A negative Faraday *A* MCD-term is expected when a hole generated by electron excitation has appropriate angular momentum.[47] Accordingly, this negative *A*-term might be produced by a transition from the accidentally degenerate ligand orbital to cobalt (LMCT) or by a transition from the degenerate cobalt orbitals to the ligand orbital (MLCT). Of the two possibilities, however, the spectra of CoAnAP support the latter possibility. This is because, as seen in the bottom of Figure 12, the first oxidation of this species is also ligand-centered, and a deformed negative Faraday *A*-term was observed, corresponding to the new absorption between the Q-band and the Soret band. Since it is very hard to consider the presence of degenerate orbitals in a monosubstituted ABBB type ligand, the possibility of the LMCT may be ruled out. Since negative Faraday *A*-term type MCD spectra were observed anyway for the ABBB and AABB type species, it is conjectured that the ligand field directly surrounding the central metal is close to D_{4h}, irrespective of the lower symmetry of the ligand.

The spectroscopic changes on reduction of $NiAn_2AP$ (Figure 13, middle) are completely different from those observed for $CoAn_2AP$ and CoAnAP (Figure 13 top and bottom), suggesting that the reduction of the latter two is occurring at the cobalt, as observed for CoPc in the same solvent.[46,48] With the progress of reduction, the Q-band and the Soret band shifted to the blue and red, respectively, while a new peak developed at ca. 490 nm for $CoAn_2AP$. In the case of $Co^{II}Pc$, the Q-band shifts to the red with the formation of $Co^{I}Pc$, and a band which has been assigned as an MLCT develops at ca. 480 nm.[46b] The above spectroscopic changes of $CoAn_2AP$ are, in this way, different from those of CoPc. Accordingly, it is premature to give a coherent interpretation on the spectra of the reduced cobalt species.

Conclusions

We have succeeded in finding a method to obtain adjacently disubstituted AABB type TAPs preferentially in a mixed condensation reaction of two types (A and B) of ortho dinitriles. The reaction is started in the presence of lithium, and the later addition of a transition metal leads to the adjacently disubstituted species. A series of these compounds and the corresponding monosubstituted ABBB type compounds have been characterized by electronic absorption and magnetic circular dichroism spectroscopies, electrochemistry, and spectroelectrochemistry, together with molecular orbital calculations.

(i) The shift and splitting (ABBB type species) or nonsplitting (AABB type species) of the Q absorption band upon ring expansion by fusion of aromatic molecules have been quantitatively analyzed experimentally by adopting simultaneous band deconvolution of the electronic absorption and MCD spectra. In ABBB type species, the Q-band shifts and splits with fusion of the aromatic rings, the extent of which increases with increasing size of the fused aromatics. Of the split Q-band, the intensity of the longer wavelength component decreases with increasing size of the fused aromatics. In AABB type species, the Q-band shifts without splitting due to the near degeneracy of the two LUMOs. We are able to adjust the Q-band position between ca. 600 and 750 nm in a stepwise manner by preparing a series of CoTAP compounds.

(ii) The redox potentials of ABBB type species appear at slightly more positive potentials than those of the corresponding AABB type species, indicating that the fused aromatic rings function as electron-releasing groups. Although the first ligand reduction potentials of these species vary slightly, the first ligand oxidation potentials show higher sensitivity to the size of the macrocycles, while the potential shifts negatively with increasing molecular size.

(iii) Both the spectroscopic results and the changes in redox potentials have been reproduced well by molecular orbital calculations within the framework of the PPP approximation. In particular, from consideration of the delocalization of the molecular orbitals obtained from the calculations, a reasonable explanation has been given to the long-standing question that the LUMO level remains almost constant while the HOMO level destabilizes with increasing size of the macrocycle. Here, since the HOMO is spreading over the whole moiety while the LUMO is localized in the central TAP core moiety, irrespective of the size of the molecule, the HOMO destabilizes while the LUMO energy is essentially fixed on ring expansion.

Acknowledgment. This research was supported by the Daiwa Anglo-Japanese Foundation and Shorai Foundation for Science and Technology to N.K., and a Grant-in-Aid for JSPS fellows to T.F. (No. 13008393).

Supporting Information Available: Mass spectroscopic calculated and observed isotope distribution patterns of all compounds in this study (PDF). This material is available free of charge via the Internet at http://pubs.acs.org.

JA012382U

(47) Michl, J. *J. Am. Chem. Soc*. **1978**, *100*, 6801; 6812.
(48) Kobayashi, N.; Lam, H.; Nevin, W. A.; Janda, P.; Leznoff, C. C.; Lever, A. B. P. *Inorg. Chem.* **1990**, *29*, 3415.